Journal of Applied Polymer Science

Preparation and performance of aramid nanofiber membrane for separator of lithium ion battery

Jinglong Li, Wenting Tian, Hongchen Yan, Lianyuan He, Xinlin Tuo
Key Laboratory of Advanced Materials (MOE), Department of Chemical Engineering, Tsinghua University, Beijing 100084, People's Republic of China
Correspondence to: X. Tuo (E-mail: tuoxl@mail.tsinghua.edu.cn)

ABSTRACT: Stable and uniform dispersions of *para*-aramid nanofibers have been prepared by adding methoxypolyethylene glycol (mPEG) in the polymerization process, followed by strong shear and dispersion. Aramid membranes are fabricated by vacuum-assisted filtration of the nanofiber dispersion and assembled into batteries as separator. The membrane properties and battery performances are characterized in detail and the effect of mPEG content on these properties is explored. It is demonstrated that aramid membranes possess good electrolyte wettability, excellent mechanical properties, and superior thermal stability, which improve the safety of lithium ion batteries. The mPEG is critical to the formation of aramid nanofibers and improves the porosity and ionic conductivity of the membranes. These fascinating characteristics and facile papermaking method endow aramid membrane potential application as separator in lithium ion batteries with superior safety. © 2016 Wiley Periodicals, Inc. J. Appl. Polym. Sci. **2016**, *133*, 43623.

KEYWORDS: batteries and fuel cells; electrochemistry; fibers; liquid crystals; nanostructured polymers

Received 19 January 2016; accepted 10 March 2016
DOI: 10.1002/app.43623

INTRODUCTION

The separator is the most critical part of lithium ion battery, which separates the positive and negative electrodes to prevent electrical short circuit while enabling free ionic transport and isolating electronic flow. The properties of the separator have a direct impact on the battery performance, such as energy density, power density, cycle life, and safety.[1] The most widely used separators in lithium ion batteries are polyolefin porous membranes, such as polyethylene (PE), polypropylene (PP), or their blends, which is attributed to their thin thickness, small pore size, and good electrochemical stability.[2–6] However, the heat resistant property of such polyolefin is not good enough, which limits its use in power batteries for the safety concerns. Their poor thermal stability will lead to thermal shrink when abnormally heated.[7] Their low mechanical property may result in mechanical rupture during battery assembly or penetration in service.[8–16] In addition, their poor compatibility with liquid electrolyte will shorten the cycle life of batteries.[17–20] Although polyolefin membranes have thermal shutdown properties, vast heat produced during the operation of lithium ion batteries will rise the internal temperature of batteries, induce the uneven distribution of heat, and even cause thermal runaway. Faced with this challenge, remarkable efforts have been made, including coating nanoparticles to enhance the interfacial stability[9,11,12,20] and exploring the nanofiber nonwovens.[16,21–25] However, the poor compatibility of inorganic particles and organic membranes still exists. Nonwoven fabric is a new method of producing separators, but it suffers from inferior mechanical strength[26] and few fibers can meet the requirement of propeties and morphologies. In conclusion, it is urgent to develop separators with improved safety performance.

The aramid fiber made of poly(*p*-phenylene terephthamide) (PPTA) is well known for thermal stability, good chemical resistance, and excellent mechanical properties, which has been widely used as reinforcement in advanced composites for aircrafts and the automotive industry and for a variety of promising applications, including bullet-proof vests, protective clothing.[27–32] However, the status of the macroscale fibers restricts the potential application as separator in lithium ion battery.[33] For example, separators made of PPTA pulp or aramid fibrid film suffer from high thickness and inferior mechanical strength. In a word, it is essential to explore microscale fibers, especially nanofibers. Aramid macroscale fibers can be split into nanofibers by dissolution in dimethylsulfoxide (DMSO) in the presence of potassium hydroxide (KOH).[34] This method has a series of disadvantages, such as low concentration, long time and low efficiency. Besides, the chemical reaction will destroy the original nature of aramid fiber with this method.

In this article, stable and uniform dispersions of aramid nanofibers are prepared by one-step method from bottom to up,

instead of the top-to-bottom approach, which consists of polymerization, spinning, and dissolution[35]. In the polymerization process of PPTA, mPEG is added to suppress the aggregation of liquid crystal PPTA chains. Aramid nanofibers are prepared with uniform size by intensive shear and precipitating agent. The mPEG contributes to increasing the dispersibility of PPTA and improving the ionic conductivity and battery performance. In addition, aramid nanofiber membranes are fabricated by self-assembly of the nanofibers by vacuum filtration. It is demonstrated that aramid nanofiber membranes possess good electrolyte wettability, excellent mechanical property, and superior thermal stability, which can be used as potential separators in high power batteries in the future.

EXPERIMENTAL

Materials

N-methyl-2-pyrrolidone (NMP) was purchased from Beijing Oriental Chemicals. China and dehydrated with water content less than 100 ppm. Calcium chloride anhydrous ($CaCl_2$) was obtained from Beijing Chemicals. China, and dried at 400 °C for 4 h in the oven before use. mPEG ($M_w = 2000$) was purchased from Xilong Chemical, China. Terephthaloyl chloride (TPC, purity 99.99%, China) and *p*-phenylene diamine (PPD, purity 99.99%, China) were purchased commercially and used as received. PP separator (Celgard 2400) was purchased from Celgard Company. Other solvents and reagents were purchased commercially and used without further purification.

Preparation of Aramid Nanofiber Membrane

NMP (100 mL) was placed in the reaction vessel and heated to 100 °C under the protection of nitrogen. Then appropriate amount of $CaCl_2$ and mPEG was slowly added to the NMP solution with magnetic stirring and heated at 100 °C for 1 h. After $CaCl_2$ and mPEG completely dissolved, a water bath was used to absorb heat in this process and cool the solution to 15 °C. Then 4.326 g (0.04 mol) PPD was added to the NMP/$CaCl_2$ solution with stirring and ice was added in the water bath to cool the solution to 0 °C. After that, 8.178 g (0.04 mol) TPC was added to this solution to react with PPD and the stirring speed was increased to 2000 r/min. The whole reaction process was carried out under a nitrogen atmosphere. When Weissenberg effect appeared, the reaction was stopped and a large amount of NMP was added to the vessel. Then the mixture was transferred to a coagulation bath of deionized water under high shear to obtain a uniform dispersion, using high shear homogenizer (wiggens D-500). The material was sucked into the head axially, then accelerated using the rotor's high rate, circumferential or peripheral velocity. The centrifugal acceleration between the outer rotor wall and the inner stator wall propelled the material through the stator shearing slits. Aramid nanofiber membranes were fabricated by self-assembly of the dispersion by vacuum-assisted filtration. Then the membranes were rinsed with deionized water to remove residual and dried in a vacuum oven. Aramid membranes with different thickness were fabricated by adjusting the amount of the fiber dispersion.

Characterization of the Aramid Nanofiber Membrane

Fourier transform infrared (FT-IR) spectra were recorded on a Nicolet Magna-IR 560 spectrometer. X-ray powder diffraction (XRD) patterns were recorded on a D/max-2200/PC (Japan Rigaku.) using CuKα radiation ($\lambda = 1.5418$ Å). The morphologies were observed by transmission electron microscopy (TEM) (Hitachi H-7650B microscope with an accelerating voltage of 80 kV). The surfaces were characterized by field emission scanning electron microscopy (FE-SEM) (Merlin Compact, Carl Zeiss, Germany).

The viscosity (η) of PPTA in 98% sulfuric acid with concentration (C) at 0.5 g/dL at 30 °C was measured using an Ubbelodhe viscometer. The inherent viscosity was obtained as following equation:

$$\eta_{inh} = \ln(\eta/\eta_0)/C \quad (1)$$

where η_0 is the viscosity of the solvent (98% sulphuric acid). The weight-average molecular weight M_w was then calculated using the following equation[36]:

$$M_w = 3902.39\eta_{inh}^{1.556} \quad (2)$$

The thickness of the membrane was calculated by taking average of multi-point measurement with micrometer caliper. The porosity of the separators was measured using n-butanol absorption method.[37] For this purpose, the mass of the separators was measured before and after immersion in n-butanol for 2 h. The porosity of the membrane was calculated by the equation:

$$\text{Porosity} = (M_w - M_d)/(\rho \times L_1 \times L_2 \times h) \times 100\% \quad (3)$$

where M_w and M_d are the mass of wet and dry membrane; ρ is the density of n-butanol; L_1 is the length of specimen; L_2 is the width of specimen; h is the thickness of specimen. Wettability was characterized by measuring the contact angle with a sessile drop method using a Dataphysics OCA-20 contact angle system. The water droplet volume was 4 μL. The measurements were carried out under ambient conditions. The electrolyte uptake was obtained by measuring the weight of separators before and after liquid electrolyte soaking for 2 h and then calculated using following equation:

$$\text{Electrolyte uptake} = (W_w - W_d)/W_d \times 100\% \quad (4)$$

where W_w and W_d are the weights of the separator before and after soaking in the liquid electrolyte, respectively.[38]

The mechanical property was investigated by universal testing machine (UTM-1432, Chengde Jinjian Testing Instrument, China). Thermal shrinkage behavior was calculated by measuring their dimensional change after heat for 0.5 h from 120 °C to 200 °C.[39] Thermal stability of the separator was evaluated by the differential scanning calorimeter (DSC) and thermal gravimetric analyzer (TGA). DSC was determined using DSC-Q2000 (TA Instruments, USA) at a temperature range from 25 °C to 300 °C at a heating rate of 10 °C/min under nitrogen atmosphere. And TGA was carried out by TGA Q5000 (TA Instrument, USA) at a temperature range from 100 °C to 800 °C at a heating rate of 5 °C/min under nitrogen atmosphere.

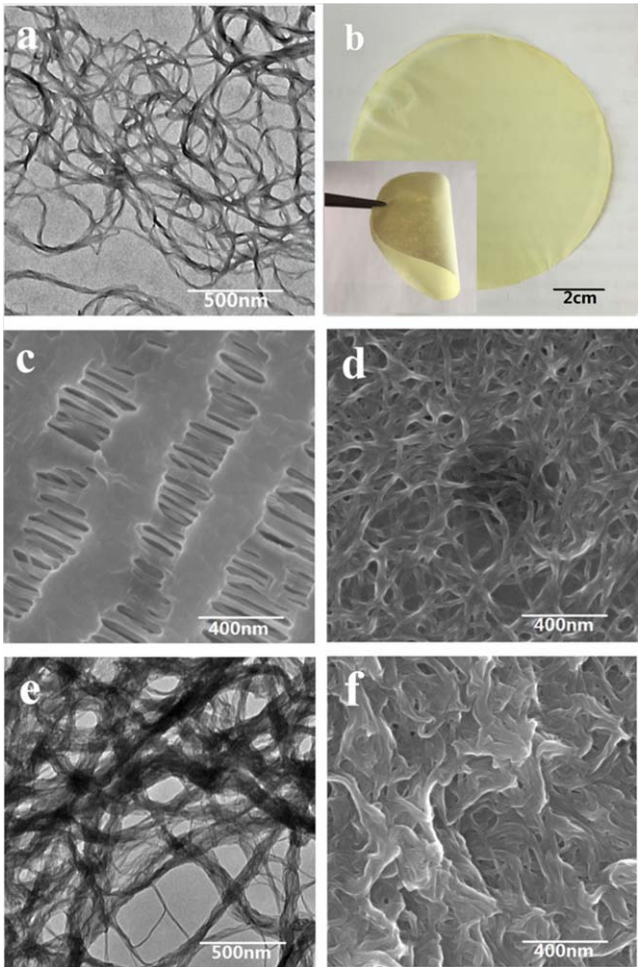

Figure 1. (a) TEM image of aramid nanofibers, (b) Photograph of the aramid membrane, (c) Typical SEM image of PP separator, (d) SEM image of the aramid membrane, (d) TEM image of pure PPTA, and (f) SEM image of pure PPTA. [Color figure can be viewed in the online issue, which is available at wileyonlinelibrary.com.]

The ionic conductivity of the liquid electrolyte-soaked separator between two stainless-steel plate electrodes was obtained by an AC impedance analysis using a CHI660E electrochemical working station over a frequency range of 1–10^5 Hz.[40] The ionic conductivity (σ) was given by the equation:

$$\sigma = L/RA \quad (5)$$

where R is the measured resistance of separator, A is the electrode area, L is the thickness of separator.[41]

C-rate capability and cycle performance of PP separator and aramid membrane were conducted over a voltage range of 2.75–4.2 V, using Land Battery Test System (Wuhan Land Electronic, China). Lithium cells (2025-type coin) were assembled by sandwiching a separator between a $LiCoO_2$ cathode and a natural graphite anode, filled with liquid electrolyte [1 *M* $LiPF_6$ in DEC/EC (1:1, v/v)]. All assembly of cells was carried out in an argon-filled glove box. Cells were charged up to 4.2 V and discharged to 2.75 V. *C*-rate capability of cells was evaluated by charging the cell at various current densities from 0.1*C* to 2*C* and discharging at the same current density with each charging. Cycle performance of cells was measured at a fixed charge/discharge current density (0.5*C*/0.5*C*).[42]

RESULTS AND DISCUSSION

Morphology and Structure Characterization

PPTA was generally synthesized by low-temperature solution polycondensation of the two monomers of PPD and TPC.[43] Different from the traditional method, the mPEG was added in this work to suppress the aggregation of liquid crystal PPTA chains in the PPTA polymerization process. The mPEG is flexible in main chain and forms hydrogen bond with PPTA, as well as partly reacts with the acyl chloride of PPTA. PPTA molecules were stabilized by mPEG and self-assembled into nanofibers. The nanofiber dispersion was obtained by strong shear in suitable media after polymerization.[44] TEM and SEM images in Figure 1 offered direct information of the obtained nanofibers with 20% mPEG added in the polymerization process. It was presented that aramid nanofibers were homogeneously distributed and the diameter ranged from 20 to 50 nm according to the addition amount of mPEG. The length of nanofibers reached tens micrometers, which was favorable to the formation of membrane with strong mechanical performance. Also, we could see from the TEM and SEM images of pure PPTA that the obtained fibers without mPEG had strong tendency to agglomerate. Aramid membranes were fabricated by vacuum-assisted filtration of the nanofiber dispersion with uniform thickness and smooth surface [Figure 1(b)]. The thickness of membranes could be adjusted by controlling the dispersion amount. As shown in Figure 1(c), the commonly used PP separator possessed uniform and slim pores, which were manufactured by uniaxially stretching process. Compared to PP separator, aramid membrane possessed three-dimensional porous network structure and highly tortuous pores, which was beneficial to absorb more electrolytes[26,45] and suppress lithium dendrites growth.[46]

Apart from the great contribution to the formation of PPTA nanofibers, it is believed that mPEG also has significant impact

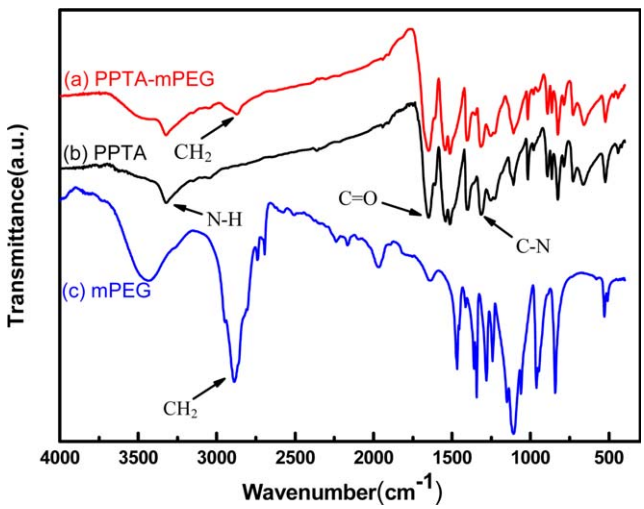

Figure 2. FT-IR spectra of (a) PPTA-mPEG, (b) PPTA, and (c) mPEG. [Color figure can be viewed in the online issue, which is available at wileyonlinelibrary.com.]

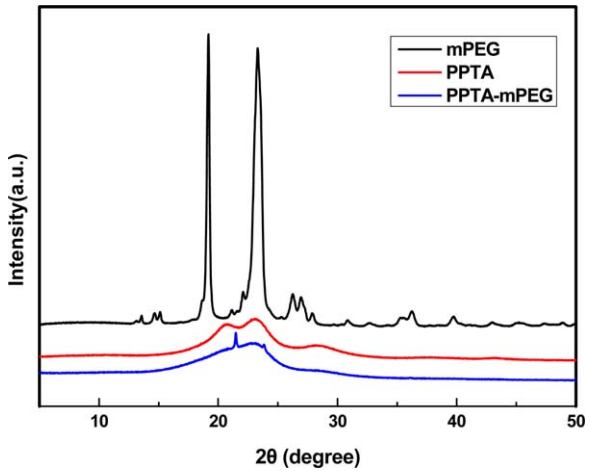

Figure 3. XRD patterns of mPEG, PPTA, PPTA-mPEG. [Color figure can be viewed in the online issue, which is available at wileyonlinelibrary.com.]

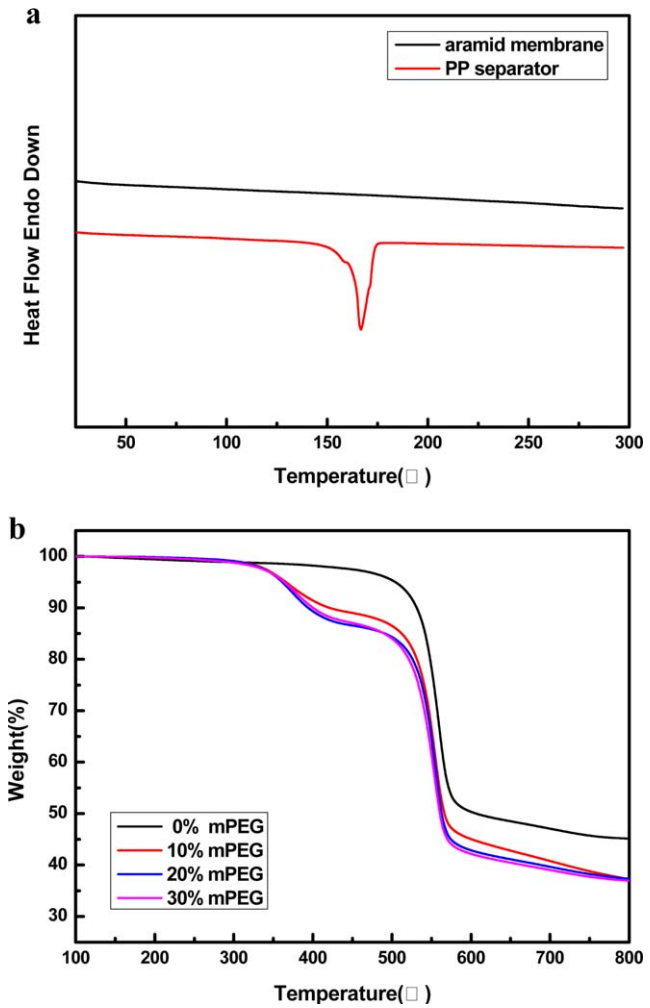

Figure 4. (a) DSC curves of PP separator and aramid membrane. (b) TGA curves of aramid membranes with different mPEG contents. [Color figure can be viewed in the online issue, which is available at wileyonlinelibrary.com.]

on the membrane properties and battery performance. Thus the state of mPEG in membrane was first studied. FT-IR spectra confirmed the introduction of mPEG into PPTA. It can be seen in Figure 2, mPEG exhibits representative peaks at 2870 and 1467 cm^{-1}, corresponding to the C-H mode, CH_2 scissoring, and waging vibrations, respectively. The peak at 1280 cm^{-1} is attributed to C-O band and the C–O–C modes of pure mPEG are located on 1059 cm^{-1}.[47] In the spectra of PPTA, the N-H stretching vibration appears at 3325 cm^{-1} and the peak at 1647 cm^{-1} can be attributed to the C = O stretching vibration, The peak at 1543 and 1511 cm^{-1} may be caused by the N-H deformation and C-N stretching coupled modes. The peak at 1250 cm^{-1} indicates the coupling vibration of N-H and C-N.[34] The PPTA-mPEG can be considered as hybrids of PPTA and mPEG. When the mPEG was decorated on PPTA, the characteristic peaks of both appeared in the PPTA-mPEG.

The phase state of mPEG in membrane was explored with XRD patterns (Figure 3). The XRD pattern of pure PPTA shows characteristic peaks at 20.8°, 22.9°, and 29.2°, corresponding to (110), (200), (004) planes, respectively.[28,29] When PPTA was functionalized by mPEG, there was a tiny peak at 21.4° and a diffuse broad band for 2θ between 20° and 30° instead of the sharp peaks at 2θ = 19° and 2θ = 23° observed in crystalline mPEG, which indicated that mPEG was amorphous in aramid membrane.[46] It is believed the crystallization of mPEG is inhibited by the nanofibers, which is favorable for ion conduction in separator.[48,49]

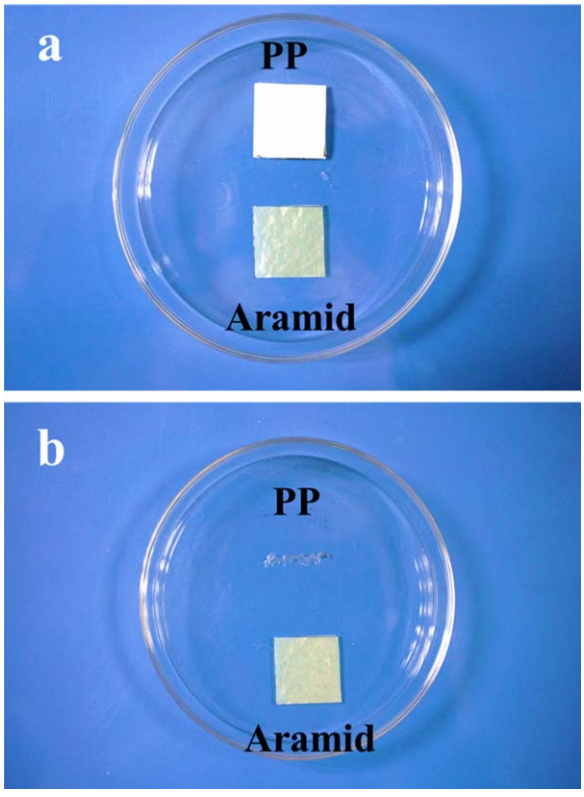

Figure 5. Photographs of PP separator and aramid membrane after heatment at (a) 120 °C (b) 200 °C for 0.5 h. [Color figure can be viewed in the online issue, which is available at wileyonlinelibrary.com.]

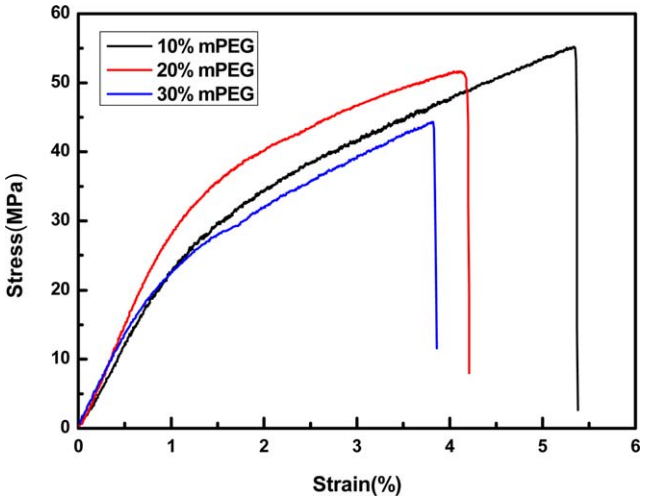

Figure 6. Stress–strain curves of aramid membranes with different mPEG contents. [Color figure can be viewed in the online issue, which is available at wileyonlinelibrary.com.]

Thermal Analysis and Mechanical Property

Aramid is famous for thermal resistance, which is important for its potential applications. For this purpose, DSC and TGA were conducted for the PP separator and aramid membranes with different compositions at nitrogen atmosphere. As we all know, PP separator tends to shrink, when the temperature rises to the softening temperature (160 °C), which will cause terrible electrical short circuit.[50] It was obtained in Figure 4(a) that aramid membrane showed no obvious endothermic peak below 300 °C, which confirmed the amorphous nature of mPEG in aramid membrane. As shown in Figure 4(b), the analysis results showed that pure aramid membrane began to decompose at about 500 °C, while aramid membrane with mPEG began to decompose at about 350 °C, which was still much higher than PP separator. This implied that the aramid membrane possessed better thermal stability than PP separator.

Thermal shrinkage of the separators was another important means of characterization of battery performance and safety. As shown in Figure 5, thermal shrinkage behavior was calculated by measuring their dimensional change after heat for 0.5 h from 120 °C to 200 °C. It was obvious that dimensional shrinkage of aramid membrane was much smaller than PP separator, which also indicated the thermal stability of aramid membrane was significantly better than that of PP separator. As we all know, superior thermal resistance could effectively prevent internal electrical short circuit and endow the battery better safety characteristic.[51]

The mechanical properties of the aramid membranes with different mPEG content were investigated. As shown in Figure 6, the tensile strength of aramid membrane was around 50 MPa with deformation about 5%, which was attributed to the stronger physical bonding between the nanofibers. Their tensile strength was isotropic owing to the random arrangement of nanofibers verified by SEM observation, which was still much higher than the transverse strength (12 MPa) of PP separator.[52] It indicated that aramid membrane could provide more reliable mechanical property for reducing the possibility of the rupture of membrane and improving the safety of the battery.

Porosity and Wettability

An appropriate porosity is necessary to hold sufficient liquid electrolyte for ionic conductivity between the electrodes. However, too high porosity will adversely impact the mechanical property, for the membrane tends to shrink as it melts and softens.[1] The porosity was measured using liquid absorption methods. As shown in Table I, the porosity of PP separator was 38.4%, while the porosity of these aramid membranes was smaller than it. The porosity increased with the increasing content of mPEG. As shown in Table II, the feed ratios of mPEG and PPTA were 10%, 20%, 30% by weight, corresponding to mPEG contents of 8.7%, 10.9%, 10.9%, respectively, which was calculated by the weight loss of mPEG in TGA curves [Figure 4(b)]. For the sake of brevity, mPEG contents herein and after refer to the feed ratios. It is noteworthy that excess addition of mPEG can no more increase the mPEG content in PPTA. However, it will influence the molecular weight of PPTA and the morphology of the nanofibers, which may subsequently affect the membrane properties and battery performance.

Separators of lithium ion battery should be wetted easily and accessible to retain the electrolyte permanently.[7] The wettability of separators was characterized by measuring the contact angle of aramid membrane with water. As shown in Figure 7, the average contact angle of PP separator was 96.4°, while that of aramid membrane was much smaller, 48.8° for aramid membrane with 10% mPEG, 45.2° for aramid membrane with 20% mPEG, 43.4° for aramid membrane with 30% mPEG, respectively. The wettability of PP separator was poor, because of its

Table I. Performance Indexes of the Separators

Samples	Thickness (μm)	Porosity (%)	Contactangle	Electrolyte uptake (%)
PP separator	25	38.4	96.4°	92
Aramid membrane (10% mPEG)	22	11.1	48.8°	143
Aramid membrane (20% mPEG)	24	18.1	45.2°	146
Aramid membrane (30% mPEG)	26	22.2	43.4°	125

Table II. Physical Properties of Aramid Membranes

Samples	mPEG:PPTA (Feed ratios, wt %)	mPEG contents (%)	η_{inh} (dL/g)	M_w ($\times 10^4$)
Aramid membrane (10% mPEG)	10	8.7	2.73	1.86
Aramid membrane (20% mPEG)	20	10.9	2.66	1.78
Aramid membrane (30% mPEG)	30	10.9	2.54	1.66

hydrophobic surface property and low surface energy.[53,54] However, aramid membrane contained hydrophilic amide and ether groups as well as porous structure and interfacial compatibility, which facilitated the process of electrolyte in battery assembly.

The electrolyte uptake was also investigated (Table I), as it could increase the cycle life of the battery. The results indicated that although the porosity of aramid membrane was smaller than PP separator, the electrolyte uptake was still higher than PP separator, thanks to its better wettability and retention ability.

Ionic Conductivity and Battery Performance

To investigate ionic conductivity, the PP separator and aramid membranes saturated with electrolyte were sandwiched between two stainless-steel electrodes and assembled in a CR2025 coin battery cell. And 150 μL of a 1 *M* $LiPF_6$ solution in an EC/DEC 1:1 v/v mixture was added to each side of the membrane as was used in other studies.[46] In this case the ionic conductivity of aramid membrane reached 0.21 mS/cm, which was lower than that of PP separator but comparable to that of some solid electrolyte such as the alkaline-dissolving aramid nanofiber/PEO membrane fabricated by layer-by-layer assembly.[46] It is worth mentioning that the temperature under actual operating conditions in a sealed battery is higher than temperature in the environment outside. Thus this value reflects the low limit of ionic conductivity. Apart from the effect of porosity, aramid membrane combined with mPEG served as an ion-conducting media, which was beneficial to the ionic conductivity.

The AC impedance spectroscopy and the ionic conductivity of the PP separator and aramid membranes were shown in Figure 8. It was interesting to find that the ionic conductivity increased as mPEG content increased (less than 20%) but decreased with higher mPEG content. As mPEG content increased, electrolyte uptake increased and the separators were more facile to ionic conduction. The thickness of obtained membranes increased slightly despite of the same weight of dispersion. There was a certain limit of the amount of mPEG reacted with PPTA and interacted with PPTA by hydrogen bond. When mPEG content was more than 20%, the mPEG content remained unchanged but the thickness of the separators increased, which led to longer path for ionic conduction and lower ionic conductivity.[42]

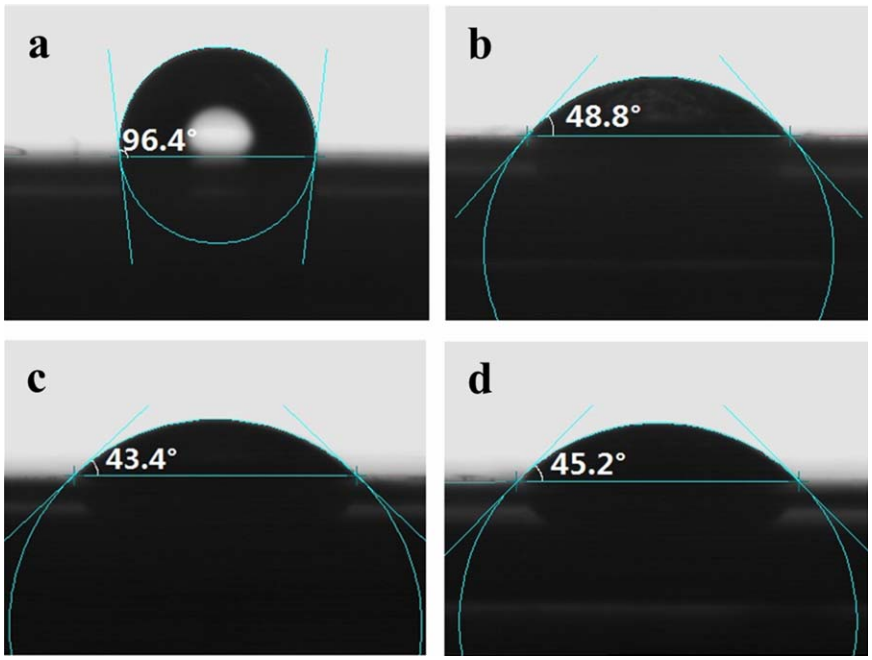

Figure 7. CCD images of contact angle: (a) PP separator, (b) aramid membrane with 10% mPEG, (c) aramid membrane with 20% mPEG, and (d) aramid membrane with 30% mPEG. [Color figure can be viewed in the online issue, which is available at wileyonlinelibrary.com.]

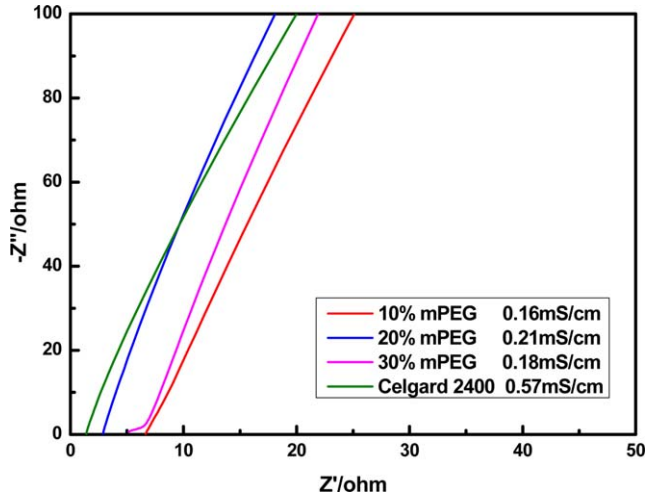

Figure 8. Electrochemical impedance spectra of aramid membranes and PP separator. [Color figure can be viewed in the online issue, which is available at wileyonlinelibrary.com.]

In order to investigate the electrochemical performance, the *C*-rate capability and cycle performance of cells assembled with PP separator and aramid membrane with 20% mPEG were examined. As shown in Figure 9, the specific discharge capacity of cells decreased gradually as current density increased, which may originate from the lower lithium diffusion rate at high current rates.[10] The specific capacity of cell using aramid membrane was comparable to that of cell using PP separator. Compared to PP separator, aramid membrane showed some worse discharging capacity at higher *C*-rates, which may be because of the lower ionic conductivity and greater thickness. It is a common sense that higher ionic conductivity is beneficial to improving the *C*-rate capability of cells.[13] And the thickness of aramid membranes was greater than PP separator, which caused lower ionic conductivity. Figure 10 depicted a comparison of the cycling performance at 0.5*C* rate for the test cells using the PP separator and the aramid membrane. The discharge capacity of cells decreased slightly with cycling because

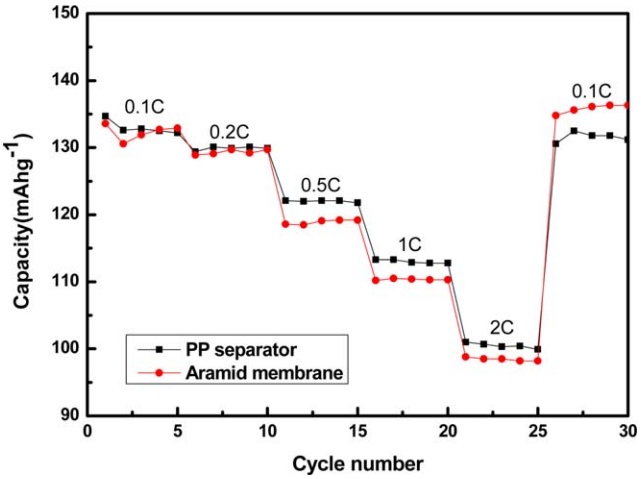

Figure 9. *C*-rate capabilities of cells assembled with PP separator and aramid membrane. [Color figure can be viewed in the online issue, which is available at wileyonlinelibrary.com.]

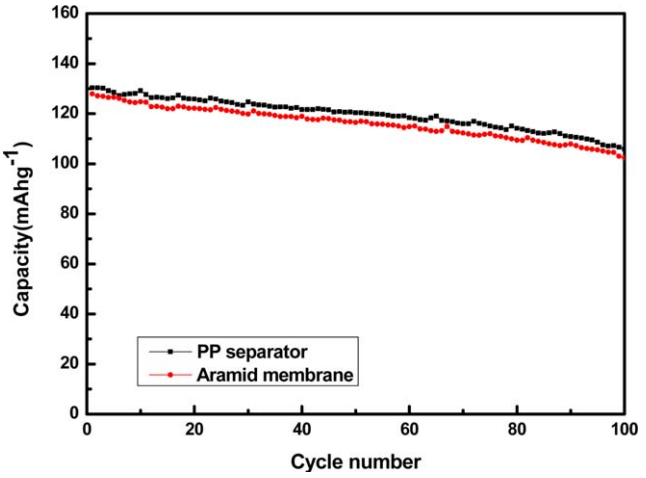

Figure 10. Cycle performance of cells assembled with PP separator and aramid membrane. [Color figure can be viewed in the online issue, which is available at wileyonlinelibrary.com.]

of the change of cell internal resistance. As the cycle number increased, physical changes occurred in the active materials and interfaces.[55] The cycle performance of cell using aramid membrane was almost comparable to that of cell using PP separator. That was because the aramid membrane possessed higher electrolyte uptake and better retention ability, despite of lower ionic conductivity. In addition, the smaller shrinkage of aramid membrane prevented the leakage of electrolytes and the better interfacial compatibility helped the separator adhere to the electrodes during cycling.

CONCLUSIONS

In conclusion, aramid nanofibers with diameters ranged from 20 to 50 nm were obtained by low-temperature solution polycondensation through a polymerization induced self-assembly process with the help of mPEG and fabricated into membrane by vacuum filtration. The mPEG plays a key role in the formation of aramid nanofibers and increasing the porosity and wettability of the membrane. Furthermore, the mPEG serves as an ion-conducting media to improve the ionic conductivity and battery performance. The aramid membrane possessed better mechanical property, thermal stability and electrolyte wettability than PP separators. All these characteristics and facile production methods provide potential application as separator for high temperature application with superior safety characteristic.

ACKNOWLEDGMENTS

This work was financially supported by the National Basic Research Program of China (2011CB606102).

REFERENCES

1. Zhang, S. S. *J. Power Sources* **2007**, *164*, 351.
2. Arora, P.; Zhang, Z. M. *Chem. Rev.* **2004**, *104*, 4419.
3. Ryou, M. H.; Lee, Y. M.; Park, J. K.; Choi, J. W. *Adv. Mater.* **2011**, *23*, 3066.

4. Venugopal, G.; Moore, J.; Howard, J.; Pendalwar, S. *J. Power Sources* **1999**, *77*, 34.
5. Rosa Palacin, M. *Chem. Soc. Rev.* **2009**, *38*, 2565.
6. Li, H.; Wang, Z.; Chen, L.; Huang, X. *Adv. Mater.* **2009**, *21*, 4593.
7. Wang, Y.; Zhan, H.; Hu, J.; Liang, Y.; Zeng, S. *J. Power Sources* **2009**, *189*, 616.
8. Jeong, H. S.; Hong, S. C.; Lee, S. Y. *J. Membrane. Sci.* **2010**, *364*, 177.
9. Jeong, H. S.; Lee, S. Y. *J. Power Sources* **2011**, *196*, 6716.
10. Kim, M.; Han, G. Y.; Yoon, K. J.; Park, J. H. *J. Power Sources* **2010**, *195*, 8302.
11. Park, J. H.; Cho, J. H.; Park, W.; Ryoo, D.; Yoon, S. J.; Kim, J. H.; Jeong, Y. U.; Lee, S. Y. *J. Power Sources* **2010**, *195*, 8306.
12. Fu, D.; Luan, B.; Argue, S.; Bureau, M. N.; Davidson, I. J. *J. Power Sources* **2012**, *206*, 325.
13. Huang, X.; Hitt, J. *J. Membrane. Sci.* **2013**, *425*, 163.
14. Zhang, S. S.; Xu, K.; Jow, T. R. *J. Solid State Electrochem.* **2003**, *7*, 492.
15. Zhang, S. S.; Xu, K.; Jow, T. R. *J. Power Sources* **2005**, *140*, 361.
16. Jeong, H. S.; Kim, J. H.; Lee, S. Y. *J. Mater. Chem.* **2010**, *20*, 9180.
17. Sohn, J. Y.; Im, J. S.; Shin, J.; Nho, Y. C. *J. Solid State Electrochem.* **2012**, *16*, 551.
18. Kim, K. J.; Kim, J. H.; Park, M. S.; Kwon, H. K.; Kim, H.; Kim, Y. J. *J. Power Sources* **2012**, *198*, 298.
19. Lee, Y. M.; Kim, J. W.; Choi, N. S.; Lee, J. A.; Seol, W. H.; Park, J. K. *J. Power Sources* **2005**, *139*, 235.
20. Choi, J. A.; Kim, S. H.; Kim, D. W. *J. Power Sources* **2010**, *195*, 6192.
21. Jeong, G.; Kim, Y. U.; Kim, H.; Kim, Y. J.; Sohn, H. *J. Energy Environ. Sci.* **2011**, *4*, 1986.
22. Jeong, H. S.; Noh, J. H.; Hwang, C. G.; Kim, S. H.; Lee, S. Y. *Macromol. Chem. Phys.* **2010**, *211*, 420.
23. Yang, C.; Jia, Z.; Guan, Z.; Wang, L. *J. Power Sources* **2009**, *189*, 716.
24. Cho, T. H.; Tanaka, M.; Ohnishi, H.; Kondo, Y.; Yoshikazu, M.; Nakamura, T.; Sakai, T. *J. Power Sources* **2010**, *195*, 4272.
25. Qi, W.; Lu, C.; Chen, P.; Han, L.; Yu, Q.; Xu, R. *Mater. Lett.* **2012**, *66*, 239.
26. Zhang, J. J.; Kong, Q. S.; Liu, Z. H.; Pang, S. P.; Yue, L. P.; Yao, J. H.; Wang, X. J.; Cui, G. L. *Solid State Ionics* **2013**, *245*, 49.
27. O'Connor, I.; Hayden, H.; Coleman, J. N.; Gun'ko, Y. K. *Small* **2009**, *5*, 466.
28. Little, B. K.; Li, Y.; Cammarata, V.; Broughton, R.; Mills, G. *ACS Appl. Mater. Interfaces* **2011**, *3*, 1965.
29. Arrieta, C.; David, E.; Dolez, P.; Vu-Khanh, T. *Polym. Compos.* **2011**, *32*, 362.
30. Bourbigot, S.; Flambard, X.; Poutch, F. *Polym. Degrad. Stabil.* **2001**, *74*, 283.
31. Rao, Y.; Waddon, A. J.; Farris, R. J. *Polymer* **2001**, *42*, 5925.
32. Rao, Y.; Waddon, A. J.; Farris, R. J. *Polymer* **2001**, *42*, 5937.
33. Fan, J. C.; Shi, Z. X.; Zhang, L.; Wang, J. L.; Yin, J. *Nanoscale* **2012**, *4*, 7046.
34. Yang, M.; Cao, K.; Sui, L.; Qi, Y.; Zhu, J.; Waas, A.; Arruda, E. M.; Kieffer, J.; Thouless, M. D.; Kotov, N. A. *ACS Nano* **2011**, *5*, 6945.
35. Flood, J. E.; White, J. L.; Fellers, J. F. *J. Appl. Polym. Sci.* **1982**, *27*, 2965.
36. Gupta, J. S.; Agge, A.; Khakhar, D. V. *Aiche J.* **2001**, *47*, 177.
37. Ding, J.; Kong, Y.; Li, P.; Yang, J. *J. Electrochem. Soc.* **2012**, *159*, A1474.
38. Hwang, K.; Kwon, B.; Byun, H. *J. Membrane. Sci.* **2011**, *378*, 111.
39. Chun, S. J.; Choi, E. S.; Lee, E. H.; Kim, J. H.; Lee, S. Y.; Lee, S. Y. *J. Mater. Chem.* **2012**, *22*, 16618.
40. Liu, X.; Kusawake, H.; Kuwajima, S. *J. Power Sources* **2001**, *97–98*, 661.
41. Ulaganathan, M.; Nithya, R.; Rajendran, S.; Raghu, S. *Solid State Ionics* **2012**, *218*, 7.
42. Liu, H. Y.; Xu, J.; Guo, B. H.; He, X. M. *J. Appl. Polym. Sci.* **2014**, *131*, 6.
43. Zhang, T.; Luo, G. H.; Wei, F.; Lu, Y. Y.; Qian, W. Z.; Tuo, X. L. *Chinese Chem. Lett.* **2011**, *22*, 1379.
44. Yan, H. C.; Li, J. L.; Tian, W. T.; He, L. Y.; Tuo, X. L.; Qiu, T. *RSC Adv.*, submitted.
45. Hao, J.; Lei, G.; Li, Z.; Wu, L.; Xiao, Q.; Wang, L. *J. Membrane Sci.* **2013**, *428*, 11.
46. Tung, S. O.; Ho, S.; Yang, M.; Zhang, R. L.; Kotov, N. A. *Nat. Commun.* **2015**, *6*,
47. Choi, B. R.; Park, S. J.; Kim, S. *J. Ind. Eng. Chem.* **2015**, *31*, 352.
48. Song, J. Y.; Wang, Y. Y.; Wan, C. C. *J. Power Sources* **1999**, *77*, 183.
49. Christie, A. M.; Lilley, S. J.; Staunton, E.; Andreev, Y. G.; Bruce, P. G. *Nature* **2005**, *433*, 50.
50. Wang, Y.; Dou, X.; Yao, Y.; Liang, Y.; Hu, J.; Zhan, H. *Text. Res. J.* **2012**, *82*, 1659.
51. Jiang, W.; Liu, Z. H.; Kong, Q. S.; Yao, J. H.; Zhang, C. J.; Han, P. X.; Cui, G. L. *Solid State Ionics* **2013**, *232*, 44.
52. Liu, Z.; Jiang, W.; Kong, Q.; Zhang, C.; Han, P.; Wang, X.; Yao, J.; Cui, G. *Macromol. Mater. Eng.* **2013**, *298*, 806.
53. Ryou, M. H.; Kim, J.; Lee, I.; Kim, S.; Jeong, Y. K.; Hong, S.; Ryu, J. H.; Kim, T. S.; Park, J. K.; Lee, H.; Choi, J. W. *Adv. Mater.* **2013**, *25*, 1571.
54. Liu, K.; Yao, X.; Jiang, L. *Chem. Soc. Rev.* **2010**, *39*, 3240.
55. Kim, D. W.; Oh, B. K.; Park, J. H.; Sun, Y. K. *Solid State Ionics* **2000**, *138*, 41.